

CMM-SolMech 2022

Shape Optimization of the Muffler Shield with Regard to Strength Properties

Joachim JAROSZ¹), Adam DŁUGOSZ²)*

¹) *Tenneco Automotive Poland sp. z o.o.*
Rybnik, Poland

²) *Department of Computational Mechanics and Engineering*
Silesian University of Technology
Gliwice, Poland

*Corresponding Author e-mail: adam.dlugosz@polsl.pl

This paper is devoted to the shape optimization of the muffler shield with regard to strength properties. Three different optimization criteria are defined and numerically implemented concerning the strength properties of the shield, and different variants of optimization tasks are solved using both built-in optimization modules and in-house external algorithms. The effectiveness and efficiency of the optimization methods used are compared and presented.

Keywords: muffler shield; evolutionary algorithms; multi-objective optimization; finite element method; optimal design.

1. INTRODUCTION

The role of the covers of the exhaust system of internal combustion engines has significantly evolved over the last years, from solely protecting the elements surrounding the system to maintaining the appropriate temperature of the exhaust gases so that certain chemical processes can take place. This applies primarily to the elimination of impurities such as nitrogen oxides, hydroxides, etc. In new-generation systems, thermal shields are installed to protect the surrounding components, mainly plastic or rubber parts, from high temperature. However, more and more often they are also used to slow down the cooling of flue gases discharged through the system.

The increasing importance of ecological factors causes the introduction of more and more restrictive emission standards. In Europe, the current EURO 6 standard requires the use of additional catalysts, such as selective catalytic reduction (SCR), to eliminate an additional portion of nitrogen oxides. These

additional components of the exhaust system require specific operating conditions to fulfill their role. One of them is the appropriate operating temperature of such a device. Optimal design for thermal characteristics concerns not only the automotive industry but also other muffler shields, such as thermoelectric generators [18].

Since the SCR is usually mounted in the middle of the system, where the exhaust gas temperature is normally much lower than directly after the engine, additional pipe covers and all parts upstream of the SCR are required to maintain the proper temperature. A higher exhaust gas temperature causes a higher temperature on the muffler jacket. Appropriately designed muffler shields are used to protect surrounding exhaust system components [13].

In order to fulfill their role, these shields must be characterized by low thermal conductivity (high thermal resistance), high emissivity, and good thermal stability (fire resistance). They should dampen vibrations very well and have high stiffness. They are usually made of heat-resistant and thin sheet metal, the thickness of which varies from 0.25 mm to even 2.5 mm.

Often the material used for their construction is aluminum or aluminized sheets. It is not uncommon to find shields made of ordinary austenitic steel. For the sake of high heat resistance, they are not damaged even at high temperatures. The air gap between the muffler shield and the rest of the exhaust system is often sufficient to maintain adequately high thermal insulation. Thermal shields come in many configurations. The simplest of them are made of a single sheet metal layer. Their main advantage is the ease of forming, but the disadvantage is that they do not effectively reduce noise and tend to vibrate (Fig. 1).

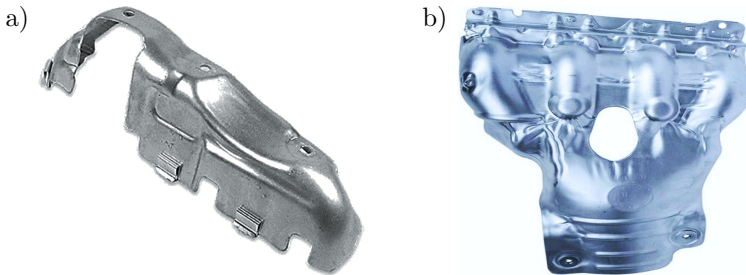


FIG. 1. Various types of single-layer muffler shields.

Therefore, some varieties used today are lined with appropriate mats resistant to high temperatures from the inside. This lining significantly improves their thermal efficiency and ability to dampen vibrations. Another type of cover is the so-called double-layer shield, consisting of two sheets of metal of different thicknesses each, with an air gap or insulating material between them. They

tend to be superior in their ability to reduce heat transfer, noise and vibration compared to the single-layer variety (Fig. 2).

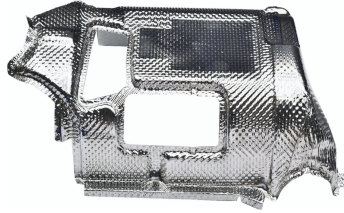


FIG. 2. Example of the geometry of the multi-layer muffler shield.

For single-layer shields, in order to reduce noise and maintain adequate stiffness, additional ribbing is introduced at appropriate locations. The shape, position or number of embossments is not obvious from a design point of view, especially if conflicting requirements often must be balanced. Optimal design of the geometric features of such embossments, including the thickness of the sheets, is the main objective of this work. Due to the larger number of design variables and the need to perform appropriate numerical simulations, it is not possible to apply classical methods of optimal design. Contemporary CAE systems have built-in optimization modules to solve this type of issue. In this paper, three optimization criteria were defined and numerically implemented with regard to the strength properties of the shield, and different variants of optimization tasks were solved using both built-in optimization modules and in-house external algorithms. Furthermore, the effectiveness and efficiency of the optimization methods used were compared and presented.

Several studies applied shape or topology optimization tasks using various optimization methods to various components in the automotive industry. For example, topology optimization was considered among others, in the works on the selected automotive suspension components [12, 17] or components of the drive unit [2, 20]. Apart from single-objective optimization [16], multi-objective optimization methods for such problems [10], or other optimization techniques such as hybrid methods were used as well [21]. Regarding the shape optimization of the muffler shields, it can be concluded that relatively few works have considered this problem [1, 14, 18]. This leads to the conclusion that the topic undertaken in this work seems both reasonable and justifiable. An additional novelty in the presented work is also the formulation and practical implementation of multi-criteria optimization tasks, as a result of which the designer receives not one but a set of Pareto-optimal solutions. In addition, the graphical representation of the results in the form of the front of Pareto optimal solutions also carries additional information for the designer about the relationship between the various criteria.

2. FORMULATION OF THE PROBLEM

The paper considers a single-layer cylindrical shield with embossing, the geometry of which is shown in Fig. 3. The shield has three mounting holes and two embossings going through its larger and smaller parts. Assuming that the diameters of the cylindrical part are imposed and fixed for technological reasons, the optimal design of the mechanical properties of this type of shield will consist of the proper shaping of the ribs while selecting the thickness of the sheet metal.



FIG. 3. Geometrical model of the muffler shield.

According to the requirements described in Sec. 1, the following criteria were formulated and numerically implemented:

- Minimization of the maximal resultant displacement of a system

$$(2.1) \quad \min_x f_1 = \max(u_{res}).$$

- Minimization of the maximal value of the equivalent stress of a system

$$(2.2) \quad \min_x f_2 = \max(\sigma_{eq}).$$

- Maximization of the lowest resonance frequency (f_{res})

$$(2.3) \quad \max_x f_3 = f_{res}.$$

The first criterion expresses the stiffness of the system, which is an important factor due to the possibility of contact between the shield and the exhaust system if the distance between these elements is not large. The second one, by reducing the maximum values of equivalent stresses determined from the Huber-Mises hypothesis, is related to the durability of the system (it should be noted that fatigue analysis was not considered). However, the third criterion allows to select the geometric features of the cover in such a way that it does not fall into resonant vibrations. Typically, such a criterion is defined as a distance between the lowest resonance frequency and the reference value. In this work, the reference value was assumed equal to 230 Hz due to the forcing frequency caused by the internal combustion engine. Considering the geometry of the shield, resonant

frequencies much lower than the reference value will not occur. Furthermore, it was assumed that it would be unfavorable for the entire exhaust system to have a frequency of 230 Hz splitting the resonant frequencies. Finally, x denotes the set of design variables described in detail below. Formulation and simultaneous consideration of more than one criterion lead to the multi-objective optimization problem [5, 11, 24].

Finite element method (FEM) was used to numerically simulate appropriate boundary value problems (BVPs) [23]. Criteria (2.1) and (2.2) are calculated based on a numerical solution of linear elastic analysis at elevated temperature [15, 19]. The FEM matrix equation of such a problem is expressed by the following formula:

$$(2.4) \quad \mathbf{K}\mathbf{U} = \mathbf{F} + \mathbf{F}_T,$$

where \mathbf{K} is the global stiffness matrix, \mathbf{U} , \mathbf{F} and \mathbf{F}_T are nodal vector of displacements, applied forces and forces due to the thermal strain vector, respectively.

Criterion (2.3) is calculated on the basis of results from the FEM modal analysis of the structural damped system

$$(2.5) \quad \mathbf{M}\ddot{\mathbf{U}} + \mathbf{C}\dot{\mathbf{U}} + \mathbf{K}\mathbf{U} = \mathbf{0},$$

where \mathbf{M} and \mathbf{C} are global mass and damping matrices, respectively.

The optimization problem involves the selection of 21 design parameters for the muffler shield consisting of the selection of design variables searching for extreme values (min or max) of defined criteria (2.1)–(2.3). Figure 4 shows the method of geometric parametrization of the model.

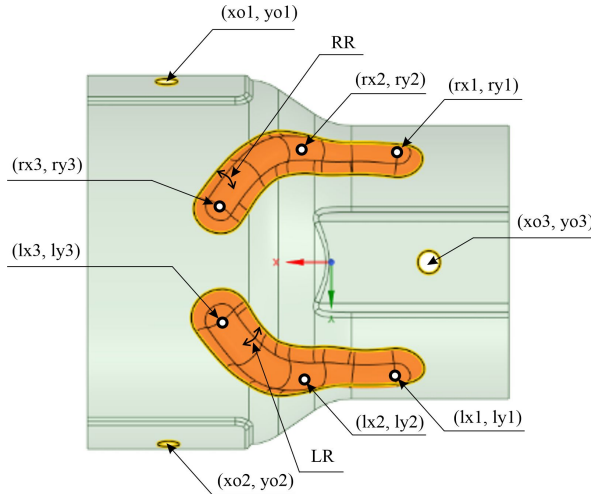


FIG. 4. Parametrization of the geometrical model.

The dimensions and position of the embossing were parameterized using seven variables (construction points of the spline curve and embossing radius). Both embossments are parametrized independently, which leads to non-symmetrical results and increasing the range of searching possibilities. Furthermore, the positions of the mounting holes and the steel sheet's thickness are the remaining parameters. In the optimization tasks, box constraints are imposed on each design variable. The range of variability for all 21 project variables is shown in Table 1, where the values are defined with regard to the global coordinate system.

Table 1. The range of variability for design parameters.

Design parameter		Box constraints		Description
		Lower	Upper	
1	xo1	4	14	Coordinates of the center of the mounting holes
2	yo1	4	36	
3	xo2	-8	19	
4	yo2	-9	2	
5	xo3	-17	10	
6	yo4	-6	5	
7	g	0.25	1	Thickness of steel sheet
8	RR	2.5	4	Embossing radius for the left and right embossing
9	LR	2.5	4	
10	rx1	-2	10	Positions of the construction points of the spline curve for the left and right embossing
11	ry1	-14	0	
12	rx2	-1	0	
13	ry2	15	16	
14	rx3	-24	-5	
15	ry3	45	65	
16	lx1	-12	0	
17	ly1	-79	-65	
18	lx2	-2	-1	
19	ly2	-52	-51	
20	lx3	5	24	
21	ly3	-20	0	

The numerical model was prepared using the ANSYS software. The shield model for a particular geometry generated in optimization tasks is built with a preponderance of elements QUAD4 type. The number of elements for variable geometry changes in a small range and is about 8500. The shield's material

is standard aluminized steel with Young's modulus of $2.1 \cdot 10^5$ MPa, Poisson's ratio of 0.3 and density of $7.85 \cdot 10^{-9}$ kg/m³. The shield is fixed at one mounting hole (point C), whereas on the other two (points A and B), initial displacement (horizontal component) equal to 0.25 mm is applied (Fig. 5). The boundary conditions imposed in such a way correspond to the actual way the shield is installed. Furthermore, a temperature gradient of $\Delta T = 60^\circ$ in entire model was assumed, resulting in constant values of the nodal force vector \mathbf{F}_T in Eq. (2.4) and no need to solve the heat conduction additionally problem.

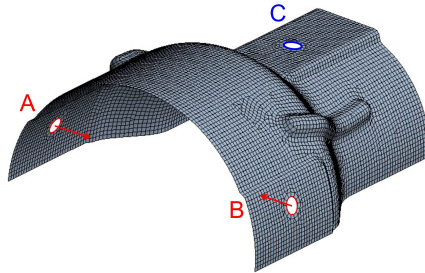


FIG. 5. Numerical model and boundary conditions.

3. APPLIED METHODS AND ALGORITHMS OF OPTIMIZATION

As mentioned in Sec. 1, different methods and algorithms are applied to solve considered optimization tasks. An external multi-criteria optimization algorithm called MOOPTIM was used. Such an algorithm has been thoroughly tested on mathematical test functions, typically used to assess the quality of performance of such algorithms (SCH, ZDT1, ZDT2, ZDT3, ZDT4, ZDT6, CONSTR, SRN, TNK) (Deb2002). Moreover, MOOPTIM was used and successfully solved different engineering problems where fitness functionals were calculated based on results from FEM simulations [3, 4, 8, 9]. MOOPTIM is an improved version of the NSGAI algorithm, among other things, with modified algorithm parameters and a selection mechanism. It significantly better solves multi-criteria optimization problems for multimodal objective functions and non-convex Pareto fronts. For other types of problems, in the majority of cases, it is competitive.

The use of an external optimization algorithm required the development and implementation of methods for automatically creating and solving boundary-value problems described by formulas (2.4) and (2.5). Figure 6 shows the method of coupling between the block of external optimization algorithm and the block of FEM computations. For each chromosome in the MOOPTIM algorithm, the geometry of the shield model is prepared. This step is utilized on the basis of the real-coded value of gens in the SpaceClaim software, for which appropriate procedures have been developed in C++ and the Python scripting language

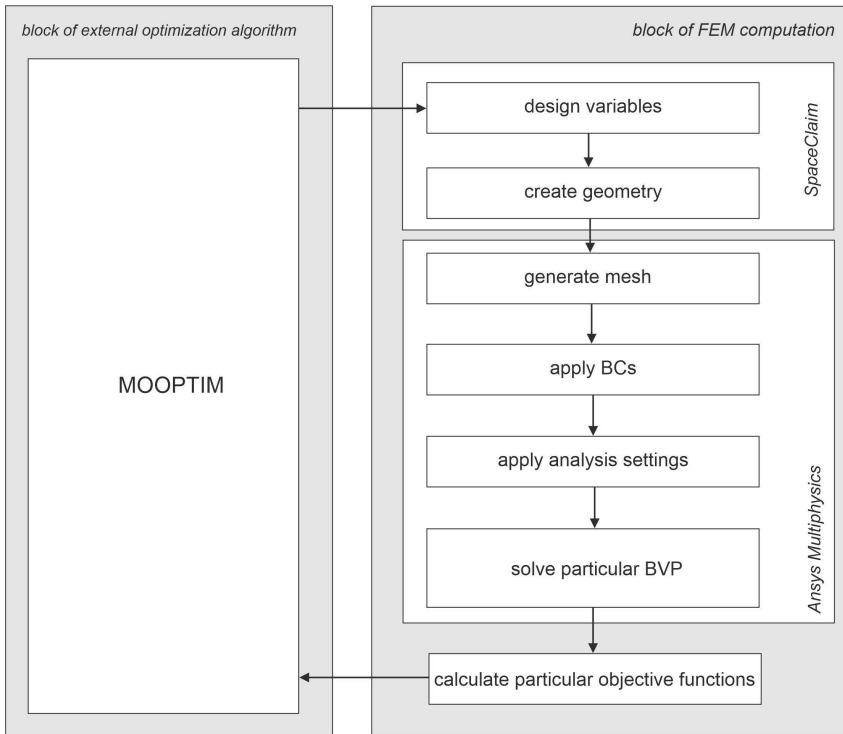


FIG. 6. General schema of the application of the external module of optimization.

(implemented in SpaceClaim). After that, mesh generation, imposing appropriate boundary condition (BC) and solving a particular boundary-value problem is solved in Ansys Software. On the basis of results files generated by Ansys, the formulated earlier objective functions are calculated by additional procedures written in C++. The optimization loop is executed until the condition of calculation termination is fulfilled.

In addition, the optimization tasks were solved using the MOGA and NSGA-II multi-criteria optimization algorithms built into Ansys software. It should be noted that both methods are not exactly prototypes of the well-known optimization methods described in the literature but only variants of them [6, 7].

4. RESULTS OF OPTIMIZATION

The optimization problems were solved as the minimization or maximization of the bi-objective tasks for previously proposed and numerically implemented objective functions. The multi-criteria optimization algorithms used in this work

exhibit the greatest effectiveness for problems in which two criteria are considered simultaneously. For more criteria considered simultaneously, accuracy and efficiency decreases. The following variants of optimization utilizing MOOPTIM, MOGA and NSGA-II were solved:

- Variant 1 – minimization of functionals (2.1) and (2.2).
- Variant 2 – minimization of functional (2.1) and maximization of functional (2.3).
- Variant 3 – minimization of functional (2.2) and maximization of functional (2.3).

For the MOOPTIM, following algorithm parameter values were used: population size – 50, number of generations 50, probability of simple crossover – 0.1, probability of arithmetic crossover – 0.1, probability of uniform mutation – 0.1, probability of Gaussian mutation – 0.1, whereas for the MOGA and NSGA-II: population size – 50, number of generations 50, convergence stability percentage – 2%, maximum allowable Pareto percentage – 70%. Such an assumption of parameter values for the external optimization procedure and the built-in algorithms in the CAE system ensures reasonable comparison considering similar computational effort (number of fitness function evaluations). Note that the user, in the case of built-in optimization algorithms, does not have access to manipulate individual parameters of the algorithm separately. The result of optimization (set of Pareto optimal solutions) utilizing all three algorithms for each considered variant is presented in Figs. 7–9.

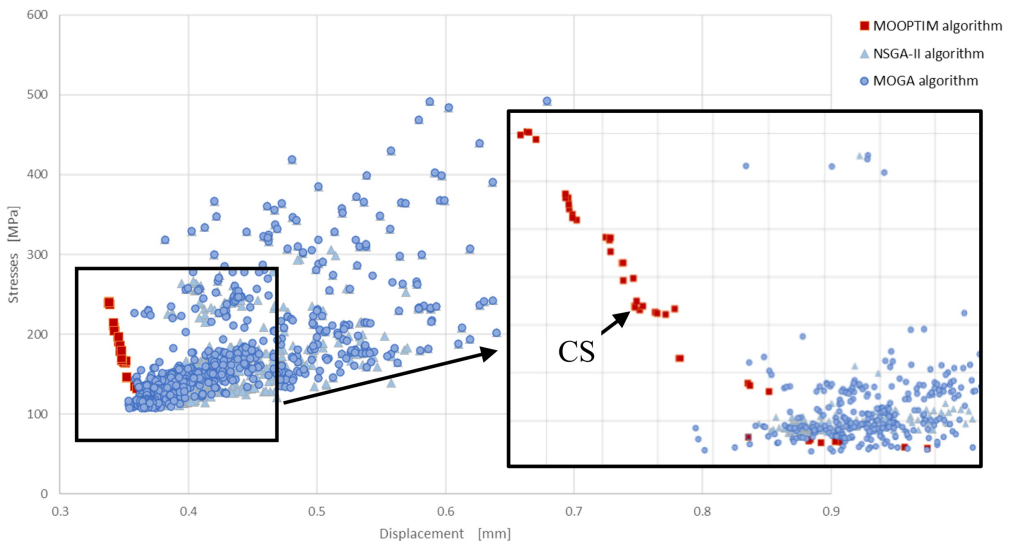


FIG. 7. Set of Pareto-optimal solutions for Variant 1.

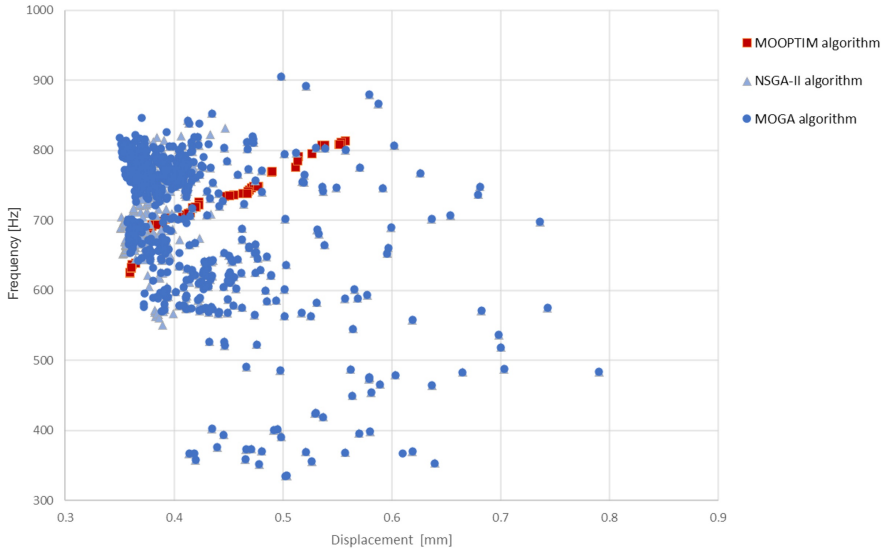


FIG. 8. Set of Pareto-optimal solutions for Variant 2.

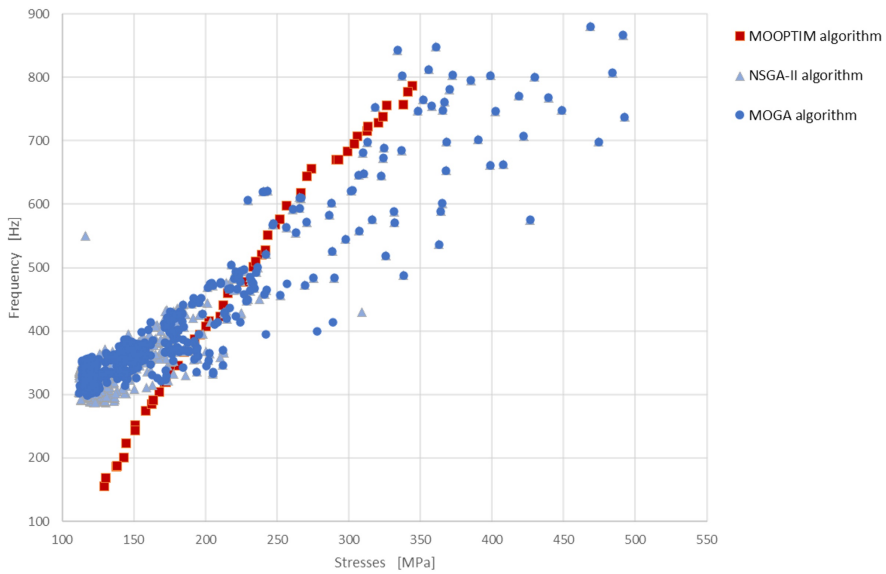


FIG. 9. Set of Pareto-optimal solutions for Variant 3.

As the solution to the above optimization tasks is not a single solution but a set of solutions, more factors should be taken into account when evaluating the quality of the resulting set, namely: the distance of found Pareto-optimal solutions from the true Pareto front (TPF), the evenness of the distribution of solutions on the Pareto front and span of the Pareto front. Assessment of

these characteristics can be conducted using a visual method, but such an assessment can be inaccurate, especially if all the features mentioned above are to be taken into account. Among several different metrics for assessing the quality of the obtained fronts, the hypervolume metric (HV) was chosen because, for the task to be solved, the location of the TPF is not known. In addition, the HV metric takes into account all three of these mentioned characteristics [22]. The calculated HV values are summarized and compared in Table 2 and Fig. 10.

Table 2. Hypervolume metric values and the number of non-dominated solutions for considered variants of optimization using MOOPTIM, MOGA and NSGA-II.

Variant	MOOPTIM		MOGA		NSGAI	
	HV	NoNS	HV	NoNS	HV	NoNS
1	179.43	33	148.22	4	171.65	8
2	425.55	50	488.98	5	485.05	13
3	230 016.7	50	258 460.8	38	272 812.1	43

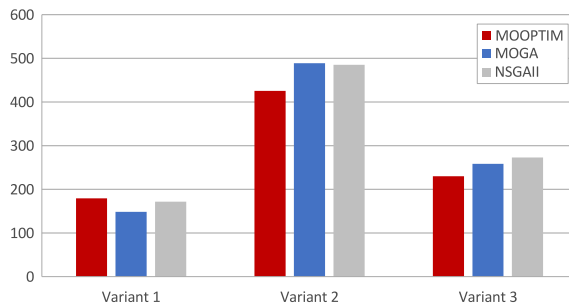


FIG. 10. Comparison of the hypervolume metric for the applied algorithms.

For the first optimization variant, the external in-house MOOPTIM algorithm was found to be superior to the built-in algorithms in the Ansys system. This is demonstrated both in Fig. 7 and by comparing the obtained HV metric values in Table 2. For Variants 2 and 3, MOGA and NSGA-II appeared to be better compared to MOOPTIM. However for the third variant, solutions obtained by MOOPTIM in some small area dominate solutions obtained by MOGA and NSGA-II. It should be noted that the Ansys optimization module presents results for multi-objective optimization tasks as a set of a collection of all solutions found so far. Such a set contains both dominated and non-dominated solutions. Based on the resulting solution sets, after exporting the data and applying the non-dominated sorting procedure, the non-dominated solutions can be displayed solely. Table 2 shows a comparison of the number of non-dominated solutions found by each of the three algorithms. For all optimization variants considered, the MOOPTIM algorithm found the largest number of

non-dominated solutions (NoNS) within the result set. On the one hand, these additional solutions require appropriate interpretation when making a decision on the final choice of the optimal solution, and on the other hand, the shape and distribution of solutions on the Pareto front bring additional information about the considered problem.

Due to limited space and in-depth discussion of the broader spectrum of Pareto-optimal solutions, only one compromise solution is presented graphically as an example. This solution was obtained for Variant 1 with the MOOPTIM algorithm (it is denoted as CS in Fig. 7) and lies closest to the utopian point (UP), which is the intersection of the axes of the coordinate system of the two criteria. Table 3 contains results (design parameters and objective functionals) of the optimization for such a solution (CS) with comparison to the initial solution (IS), graphically presented in Fig. 4 and Fig. 5 but simulated for different values of the steel sheet thickness.

Table 3. Comparison of optimization results for selected compromise solutions and the different cases of initial solutions.

Solution	DP1	DP2	...	DP7 (g) [mm]	...	DP20	DP21	f_1 [mm]	f_2 [MPa]	f_3 [Hz]
IS	9.0	25.0	...	0.25	...	5.0	-20.0	0.61	195.5	303.4
	9.0	25.0	...	0.50	...	5.0	-20.0	0.58	310.7	501.1
	9.0	25.0	...	0.75	...	5.0	-20.0	0.57	399.2	659.3
	9.0	25.0	...	1.00	...	5.0	-20.0	0.56	468.2	799.4
	9.0	25.0	...	0.46	...	5.0	-20.0	0.59	294.3	476.2
CS	4.6	12.0	...	0.46	...	5.4	-13.6	0.34	166.2	516.9

As can be seen for the IS, as the thickness of the plate increases, the stiffness increases – criterion (2.1) decreases, but the maximum stresses and the first resonance frequency also increase. The application of the proposed and developed optimization methods in the work made it possible to find a compromise solution for which it was possible to significantly improve criteria (2.1) and (2.2) and to find the value of the third criterion (2.3) for which the value of the first resonant frequency is at a safe distance from the assumed extinction frequency, described in Sec. 2. The compromise solution obtained is characterized by asymmetry, both of the embossing and the location of the upper mounting hole. Figure 11 presents the geometry (front and top view) for the optimal CS. The penultimate row of Table 3 contains values for a solution geometrically identical to the initial one but with a sheet thickness equal to the selected compromise solution obtained. Comparing these solutions, improvements can be seen for all three functionals. Figure 12 contains color maps of equivalent von Mises stresses for these solutions.

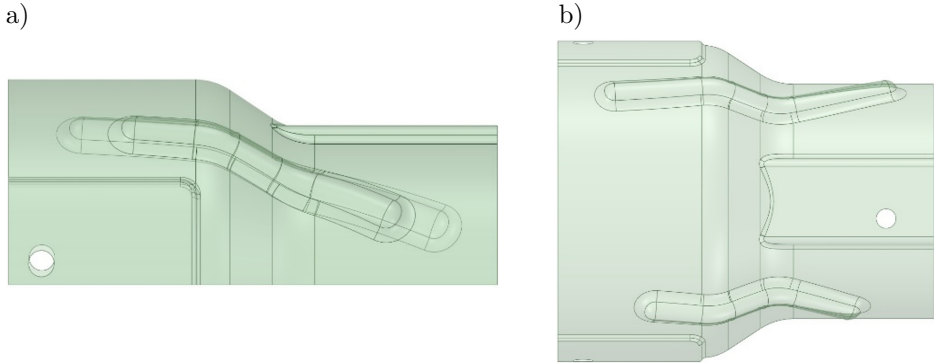


FIG. 11. Geometry of the muffer shield for the selected compromise solution.

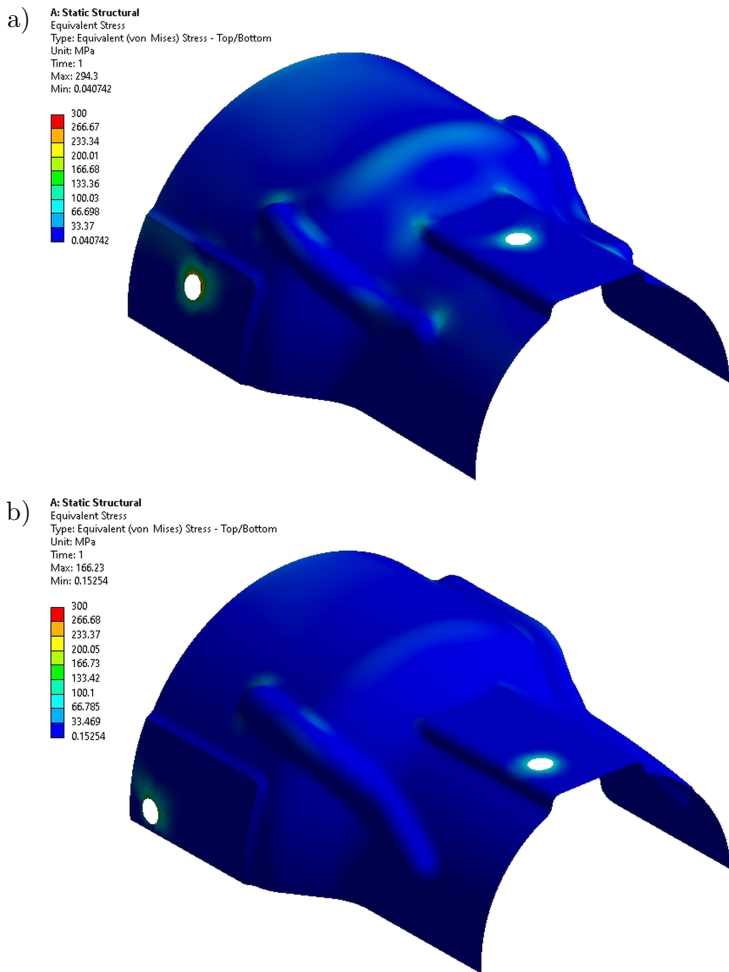


FIG. 12. Distribution of the equivalent stresses in the model for the selected compromise solution.

5. FINAL REMARKS

A method of shape optimization of the muffler shield with regard to strength properties was presented. The in-house multi-criteria optimization algorithm MOOPTIM used in this paper is a good alternative to the built-in optimization algorithms. Considered functionals are typically contradictory, so applying a multi-objective evolutionary algorithm based on the Pareto concept is a good choice. The proposed approach goes beyond just using CAE's built-in optimization algorithms. Using an external optimization algorithm requires, admittedly, the development of in-house parametrization and calculation of fitness functional procedures; however, it significantly increases the capabilities of solving optimization tasks. Although in the example presented in the paper, MOOPTIM did not perform better than the built-in algorithms; however, this does not have to be the same for other examples or problems. The proposed approach makes it possible to accurately determine the parameters of the optimization algorithm. As mentioned in Sec. 4, for more criteria considered simultaneously (greater than 3), the accuracy and efficiency of algorithms such as NSGA-II decrease. Improved versions of multi-criteria optimization algorithms can be used in such cases with the presented method. There is nothing to prevent using a similar approach for single-criteria tasks even if they are particularly difficult to optimize (for example, due to the existence of a very large number of local minima). Defining other criteria can be relatively easily implemented as well.

ACKNOWLEDGMENTS

The research was partially co-financed under grant no DWD/3/7/2019 supported by the Ministry of Science and Education in Poland and a statutory subsidy of the Faculty of Mechanical Engineering, Silesian University of Technology.

REFERENCES

1. AMINUDDIN J., WIHANTORO, BILALODIN, SUNARDI, RAUF N., Designing of muffler part for car exhaust system with low emission and noise using conjugate gradient method, *Journal of Physics: Conference Series*, **1494**(1): 012041, 2020, doi: 10.1088/1742-6596/1494/1/012041.
2. BARBIERI S.G., GIACOPINI M., MANGERUGA V., MANTOVANI S., A design strategy based on topology optimization techniques for an additive manufactured high performance engine piston, *Procedia Manufacturing*, **11**: 641–649, 2017, doi: 10.1016/j.promfg.2017.07.162.

3. BELUCH W., DŁUGOSZ A., Multiobjective global optimization of mechanical systems with cracks, *Journal of Theoretical and Applied Mechanics*, **58**(2): 553–564, 2020, doi: 10.15632/jtam-pl/119092.
4. BURCZYŃSKI T., KUŚ W., BELUCH W., DŁUGOSZ A., POTERAŁSKI A., SZCZEPANIK M., *Intelligent Computing in Optimal Design, Solid Mechanics and Its Applications*, Vol. 261, Springer International Publishing, 2020, doi: 10.1007/978-3-030-34161-9.
5. COLLETTE Y., SIARRY P., *Multiobjective Optimization: Principles and Case Studies*, Springer, 2003.
6. DEB K., Multi-objective genetic algorithms: problem difficulties and construction of test problems, *Evolutionary Computation*, **7**(3): 205–230, 1999, doi: 10.1162/evco.1999.7.3.205.
7. DEB K., PRATAP A., AGARWAL S., MEYARIVAN T., A fast and elitist multi-objective genetic algorithm: NSGA-II, *IEEE Transactions on Evolutionary Computation*, **6**(2): 181–197, 2002, doi: 10.1109/4235.996017.
8. DŁUGOSZ A., Multiobjective evolutionary optimization of MEMS structures, *Computer Assisted Methods in Engineering and Science*, **17**(1): 41–50, 2010.
9. DŁUGOSZ A., Optimization in multiscale thermoelastic problems, *Computer Methods in Materials Science*, **14**(1): 86–93, 2014.
10. EBRAHIMI-NEJAD S., KHEYBARI M., BORUJERD S.V.N., Multi-objective optimization of a sports car suspension system using simplified quarter-car models, *Mechanics & Industry*, **21**(4): 412, 2020, doi: 10.1051/meca/2020039.
11. FONSECA C.M., FLEMING P.J., An overview of evolutionary algorithms in multiobjective optimization, *Evolutionary Computation*, **3**(1): 1–16, 1995, doi: 10.1162/evco.1995.3.1.1.
12. GARDEA A.M., VALENZUELA J.C.M., Topological optimization of automotive structures under impact using robust design, *Computer-Aided Design and Applications*, **12**(sup1): 33–47, 2015, doi: 10.1080/16864360.2015.1077073.
13. IKPE A.E., KELLY O.E., ABDULSAMAD G., Engineering material selection for automotive exhaust systems using CES Software, *International Journal of Engineering Technologies*, **3**(2): 50–60, 2017, doi: 10.19072/ijet.282847.
14. JAGDEESH H.K., MANJUNATHA K., REDDY M., Numerical and experimental investigation on thermal behavior of exhaust heat shield, *International Journal of Innovative Science, Engineering & Technology*, **2**(11): 30–33, 2015.
15. KLEIBER M., *Handbook of Computational Solid Mechanics – Survey and Comparison of Contemporary Methods*, Springer-Verlag, Berlin, 2011.
16. KNAPCZYK J., MANIOWSKI M., Optimization of 5-rod car suspension for elastokinematic and dynamic characteristics, *Archive of Mechanical Engineering*, **57**(2): 133–147, 2010, doi: 10.2478/v10180-010-0007-x.
17. KONG Y.S., ABDULLAH S., OMAR M.Z., HARIS S.M., Topological and topographical optimization of automotive spring lower seat, *Latin American Journal of Solids and Structures*, **13**(7): 1388–1405, 2016, doi 10.1590/1679-78252082.
18. LIU X., DENG Y.D., CHEN S., WANG W.S., XU Y., SU C.Q., A case study on compatibility of automotive exhaust thermoelectric generation system, catalytic converter and muffler, *Case Studies in Thermal Engineering*, **2**: 62–66, 2014, doi: 10.1016/j.csite.2014.01.002.
19. LURIE A.I., *Theory of Elasticity*, Springer-Verlag, Berlin, 2005.

20. MUHAMMAD A., ALI M.A.H., SHANONO I.H., Design optimization of a diesel connecting rod, *Materials Today Proceedings*, **22**(Part 2): 1600–1609, 2020, doi: 10.1016/j.matpr.2020.02.122.
21. SEBASTJAN P., KUŚ W., Hybrid shape optimization of automotive spring seat, *International Journal of Automotive Technology*, **23**(4): 957–965, 2022, doi: 10.1007/s12239-022-0083-1.
22. WHILE L., HINGSTON P., BARONE L., HUBAND S., A faster algorithm for calculating hypervolume, *IEEE Transactions on Evolutionary Computation*, **10**(1): 29–38, 2006, doi: 10.1109/TEVC.2005.851275.
23. ZIENKIEWICZ O.C., TAYLOR R.L., *The Finite Element Method*, vol. 1–3, Butterworth, Oxford, 2000.
24. ZITZLER E., THIELE L., Multiobjective evolutionary algorithms: A comparative case study and the strength Pareto approach, *IEEE Transactions on Evolutionary Computation*, **3**(4): 257–271, 1999, doi: 10.1109/4235.797969.

Received December 23, 2022; accepted version June 7, 2023.



Copyright © 2023 The Author(s).

This is an open-access article distributed under the terms of the Creative Commons Attribution-ShareAlike 4.0 International (CC BY-SA 4.0 <https://creativecommons.org/licenses/by-sa/4.0/>) which permits use, distribution, and reproduction in any medium, provided that the article is properly cited. In any case of remix, adapt, or build upon the material, the modified material must be licensed under identical terms.